Wearable Magnetic Field Sensors for Flexible Electronics

Michael Melzer, Jens Ingolf Mönch, Denys Makarov, Yevhen Zabila, Gilbert Santiago Cañón Bermúdez, Daniil Karnaushenko, Stefan Baunack, Falk Bahr, Chenglin Yan, Martin Kaltenbrunner, and Oliver G. Schmidt*

The flourishing and eagerness of portable consumer electronics necessitates functional elements to be lightweight, flexible, and even wearable.[1–7] Flexible devices advance from interconnects and individual sensing elements toward complex platforms consisting of communication and diagnostic components that fuel the vision of creating multifaceted, interactive,[8] and wearable electronics.[9]

Next generation flexible appliances aim to become fully autonomous and will require ultra-thin and flexible navigation modules, body tracking, and relative position monitoring systems. Such devices fulfill the needs of soft robotics,[10,11] functional medical implants[12,13] as well as epidermal,[9,14] imperceptible,[15,16] and transient[17,18] electronics. Magnetic field sensors offer the possibility to sense and respond to external magnetic fields, which are considered as a vital feature when integrated into these novel kinds of electronic devices. Magnetosensorics is a versatile tool to assess mechanical movements not only in artificial devices like robotics but also in vivo. Foreseeable applications include real time monitoring of artificial joints or valves of the heart to diagnose early stages of dysfunctions. Key building blocks of navigation and position tracking devices are Hall effect sensors. Unfortunately, conventional semiconductor-based Hall sensors are about 400-µm-thick and rigid, limiting their direct applicability in flexible electronics.

Here, we introduce a technology platform that allows us to fabricate highly flexible magnetic field sensors relying on the Hall effect. We combine inorganic functional nanomembranes with polymeric foils to achieve flexible sensing elements with a near bulk sensitivity of about –2.3 V $(AT)^{-1}$. The flexible sensors fabricated on 100-µm-thick polyimide foils withstand severe mechanical deformations. We observe only a minor reduction in the sensor performance when bent into a radius of 6 mm, which is fully recovered in the flat state.

We chose 100-µm-thick polyimide (PI) and 25-µm-thick polyether ether ketone (PEEK) foils to demonstrate the viability of our technology platform. Hall sensor elements are formed by depositing bismuth films via magnetron sputtering onto the PI and PEEK supports. These materials reveal exceptionally good mechanical, thermal, and chemical stability and are applied in state of the art consumer electronics. Bismuth-based Hall sensors[19–22] bear several distinct advantages: i) Bi has the largest Hall coefficient of $-(5–6) \times 10^{-5}$ V cm $(AT)^{-1}$[23] and thus the largest sensitivity among all (half-) metals,[24] ii) the use of Bi allows surface depletion effects relevant for miniaturized semiconducting micro-Hall probes to be overcome; hence, Hall sensors with a sub-µm lateral size operating at room temperatures have been fabricated using Bi thin films,[19,20] and iii) Bi is readily processed using standard microelectronic facilities. Here, we deposit bismuth films onto electrical contacts, which are prepared on flexible foils (see Experimental Section for details). The resulting sensors can be bent on demand after their fabrication (**Figure 1**a).

Adhering the flexible sensor to a finger (Figure 1b), creates an interactive pointing device and builds a component for wearable electronics (Figure 1c). By monitoring the sensor output, we visualize the relative position of the finger with respect to a permanent magnet (compare Figure 1d and e). Details on the conditioning electronics used here can be found in Figure S1 in the Supporting Information. Fabricated in this way, magnetic field sensing elements extend our cognition to magnetic fields that by no means can be detected by human beings. Such a concept

M. Melzer, Dr. J. I. Mönch, Dr. D. Makarov, G. S. Cañón Bermúdez, D. Karnaushenko, Dr. S. Baunack, Prof. C. Yan, Prof. O. G. Schmidt
Institute for Integrative Nanosciences
Institute for Solid State and Materials Research Dresden (IFW Dresden)
01069, Dresden, Germany
E-mail: d.makarov@ifw-dresden.de

Dr. Y. Zabila
The H. Niewodniczański Institute of Nuclear Physics
Polish Academy of Sciences
31–342, Krakow, Poland

F. Bahr
Elektrotechnisches Institut
Technische Universität Dresden
01069, Dresden, Germany

Prof. C. Yan
College of Physics
Optoelectronics and Energy & Collaborative Innovation Center of Suzhou Nano Science and Technology
Soochow University
215006, Suzhou, China

Dr. M. Kaltenbrunner
Department of Soft Matter Physics
Johannes Kepler University
Altenbergerstrasse 69
4040 Linz, Austria

Prof. O. G. Schmidt
Material Systems for Nanoelectronics
Chemnitz University of Technology
09107 Chemnitz, Germany

Prof. O. G. Schmidt
Center for Advancing Electronics Dresden
Dresden University of Technology
01062 Dresden, Germany

DOI: 10.1002/adma.201405027

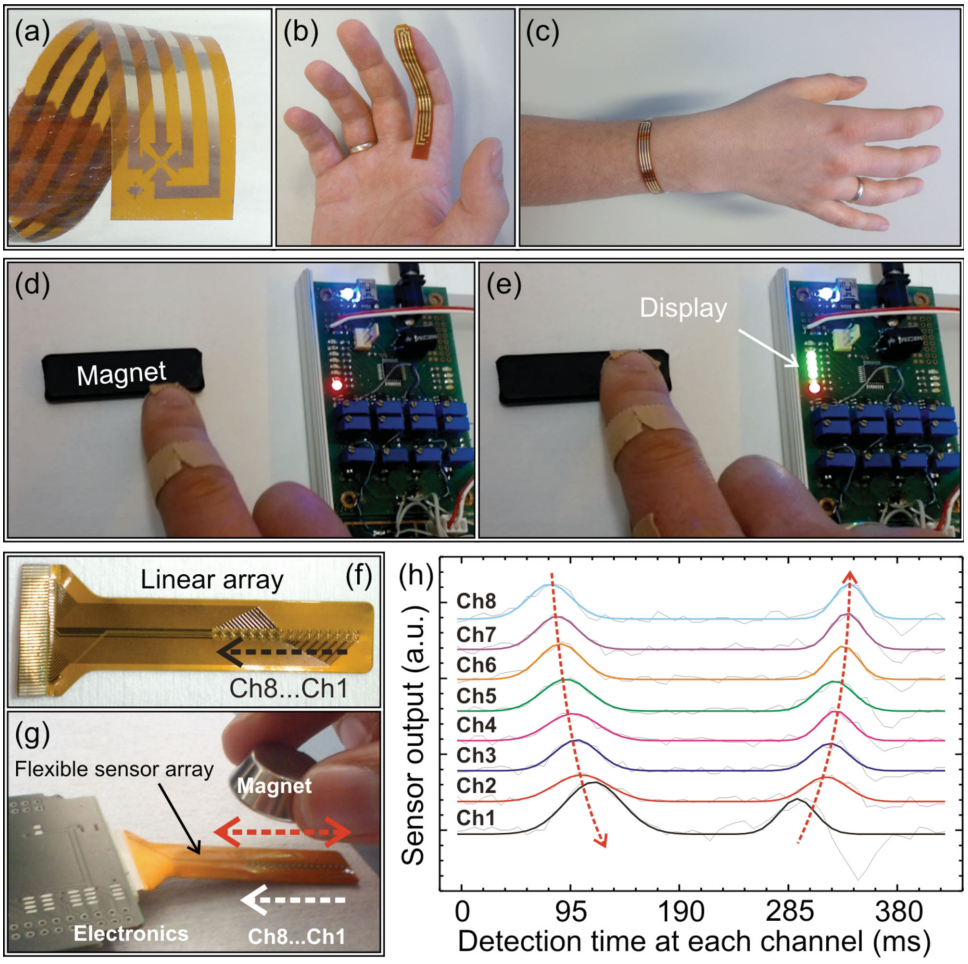

Figure 1. a) Magnified view of the flexible Hall sensor head. The sensor can be mounted on a finger (b) or located at the wrist of a hand (c). d-e) An interactive pointing device is fabricated by applying the flexible sensor to the finger. The relative position of the finger with respect to a permanent magnet is displayed in real time by monitoring the sensor output. f) 1-Dimensional linear array of 8 Hall sensors on an FPC. g) Flexible linear array of sensors connected to the read-out electronics. The sensors are exposed to the field of a permanent magnet, which is swept along the sensor array. h) Time evolution of the response at each of 8 sensors (channels 1 to 8) upon sweeping the magnet from channel 8 to 1 and back. The maximum on the curve corresponds to the arrangement when the magnet is located above the respective sensor in the array.

is beneficial, for instance for safety applications where objects located in a dangerous environment that do not permit direct access by hand can be manipulated, or where unobtrusive and robust magnetic beacons can warn of imminent health risks.

In addition to single sensors providing a point-like measurement of the magnetic flux density, we prepared 1D linear (Figure 1f) and 2D sensor arrays on commercial 150-µm-thick double layer flexible printed circuit (FPCs) boards, which defines the Hall-cross contact geometries and sensor arrangements. These sensor arrays can be applied to reconstruct a spatial and/or temporal profile of the magnetic field. For demonstration purposes, we exposed the flexible sensors array consisting of eight bismuth Hall sensors to the field of a permanent magnet (Figure 1g), which is swept forth and back along the sensor array. The maximum signal is achieved when the magnet is located above the respective sensor in the array (Figure 1h). Hence, by monitoring the shift of the maximum for each of the eight sensors, we can access the transient information on the evolution of the external magnetic field; in this particular case, we measure the displacement of a magnet as a function of time. This feature can be useful to monitor the magnetic field profile across a nonplanar area, e.g., the stator pole of an electrical machine to minimize losses and improve its overall efficiency (Figure S2 and S3, Supporting Information).

In order to optimize the Hall performance of the flexible sensors, namely, the Hall sensitivity, a series of samples was prepared, where Bi films with different thicknesses in the range between 65 and 2000 nm were deposited onto flexible PEEK and PI foils. In addition, reference samples with nominally the same layer stack were prepared on rigid glass and Si substrates for comparison studies. Annealing is known to strongly influence the polycrystalline structure and hence the magnetoelectrical properties of deposited bismuth thin films.[25,26] Therefore, thermal treatment was applied to the sensors in order to determine the correct growth conditions that result in optimal Hall performance. Here, Bi films were deposited at substrate temperatures ranging from room temperature (RT) to 150 °C. Furthermore, post-fabrication annealing of the samples

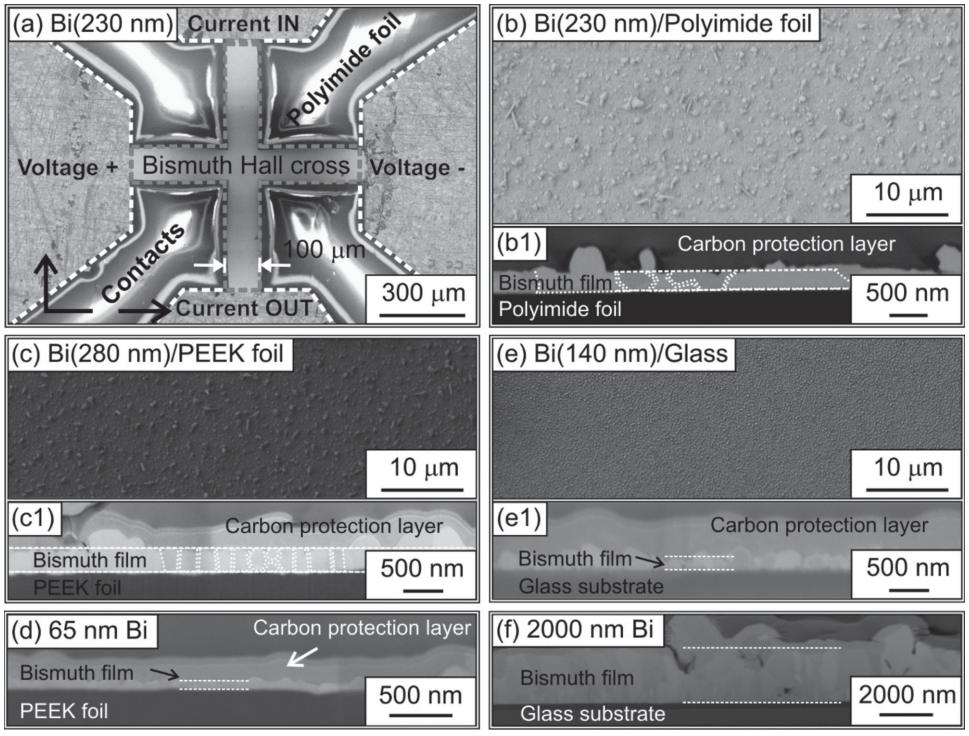

Figure 2. a) Overview SEM image taken at the location of the Hall cross prepared at room temperature on the polyimide foil and subsequently post-annealed at 250 °C for 3 h. Electrical contacts are indicated in the image as well. The sensor element consists of a 230-nm-thick Bi layer. b) Magnified view of panel (a) revealing the morphology of the top surface of the Bi layer. c) SEM image of the top surface of the 280-nm-thick Bi film on flexible PEEK foil. e) Top view of the 140-nm-thick Bi on rigid glass. The panels (b1), (c1), and (e1) show the cross-section images of the respective samples prepared by FIB milling. Panels (d) and (f) reveal cross-section of the samples with 65- and 2000-nm-thick Bi, respectively.

prepared at RT on polyimide foils was carried out at 250 °C for 3 h in air. The optimized Bi films with a thickness of 250 nm were lithographically patterned in the conventional Hall geometry as shown in Figure 1a and **Figure 2**a with an active area of the Hall sensor of 100 μm × 100 μm. Details on the patterning process can be found in the Experimental Section.

Structural characterization using scanning electron microscopy (SEM) of the samples is shown in Figure 2. The overview image revealing the location of the 230-nm-thick bismuth Hall sensor annealed at 250 °C for 3 h is presented in Figure 2a showing the Hall cross as well as the position of electrical contacts. A magnified top view image taken at the Bi film is shown in Figure 2b. Note that the morphologies of the Bi layers grown on PEEK and polyimide foils are very similar (compare Figure 2b and 2c), indicating that the growth is almost independent of the choice of the polymeric substrate. The sample on PEEK foil is prepared without an additional post-fabrication annealing step and therefore exhibits a smaller lateral size of the Bi grains. The comparison of the top view images taken of the samples prepared on polymeric foils and rigid glass substrates suggests a more grainy morphology of the Bi functional layer prepared onto a flexible foil (compare Figure 2b, 2c, and 2e). To study the morphology in more detail, cross-sectional SEM images were taken. The cross-section cut is prepared using focused ion beam (FIB) etching in a dual-beam station. For these investigations, the samples were additionally covered with a carbon layer. In contrast to the information provided by the top view images, the cross-section study reveals better film quality at the local scale for samples prepared on polymeric membranes. Bismuth grains are regular and firmly in contact with each other, suggesting a good electrical conductivity of the samples. In agreement with reports on Bi growth on rigid substrates,[26] the additional annealing step results in a substantial increase of the grain size to (860 ± 390) nm (on polyimide, Figure 2b1) as compared to the (180 ± 50) nm (on PEEK, Figure 2c1). The increase of the size of the Bi crystallites is expected to improve the Hall performance of the sensor elements as there will be less electron scattering events at the grain boundaries. However, at a larger scale of several micrometers, thicker grains can be clearly identified (compare Figure 2b1, 2c1 and 2e1). The presence of these sparsely distributed larger grains is not expected to adversely influence the overall electrical conductivity of the sample.[22] The decrease of the Bi film thickness down to 65 nm results in a substantial increase of the granularity of the film with the appearance of voids (Figure 2d), which causes an increase of the overall sample resistance (see discussion below and Figure S4, Supporting Information). In contrast, when the thickness of the functional layer increases (Figure 2f), the crystallites grow in size and form a continuous layer.

The magneto-electrical performance of the Bi-based Hall sensors prepared on flexible foils was characterized by measuring the Hall resistance of the samples positioned between the poleshoes of an electromagnet. Measurements were carried out at room temperature. The sensor sensitivity is defined as the slope of the Hall response (Hall voltage vs magnetic flux

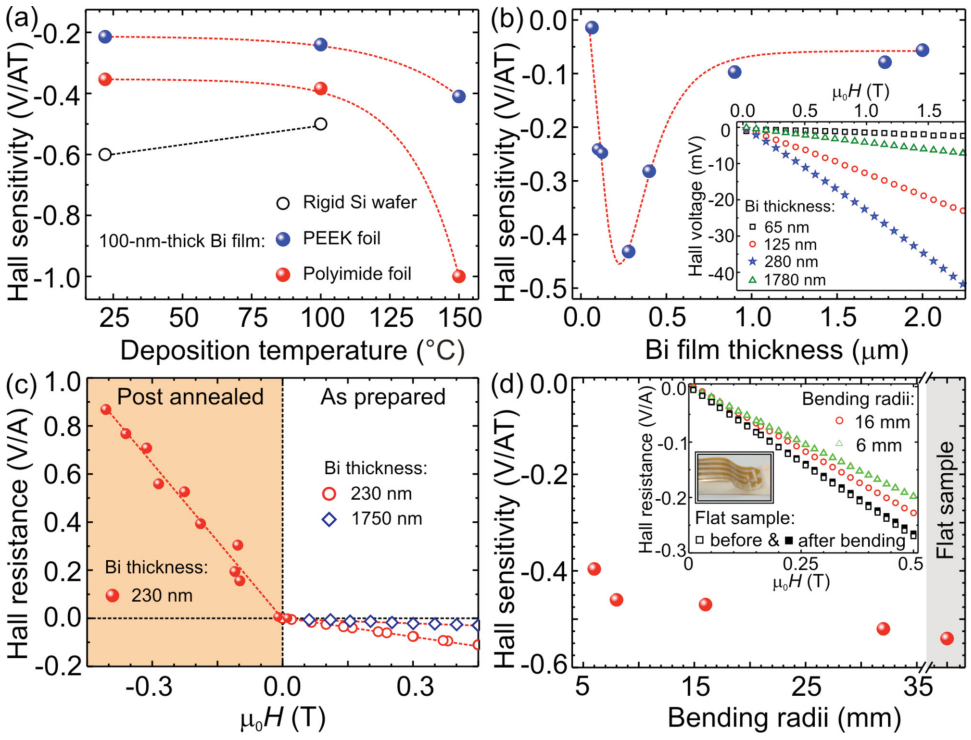

Figure 3. Performance of the flexible Hall sensors. a) Hall sensitivity of the 100-nm-thick Bi film grown onto flexible PEEK and polyimide foils measured on the samples prepared at different temperatures. Respective data for the samples prepared on rigid Si wafers is shown for comparison. b) Impact of the Bi film thickness on the Hall sensitivity for the sensors prepared at RT on PEEK foils. The inset shows the change of the Hall voltage with a magnetic flux density of the sensor elements as a function of the Bi film thickness. The measurement was carried out with a supply current of 50 mA. c) Change of the Hall resistance with magnetic flux density measured of the 230-nm-thick Bi film prepared on a polyimide foil. A comparison of the Hall characteristics of the as-prepared and post-annealed samples is shown in the right and left panels, respectively. Post-annealing was performed at 250 °C for 3 h. Right panel shows the Hall resistance of the samples of different thickness. Dashed lines are a guide to the eye. d) Variation of the Hall resistance of flexible sensors upon bending. The sensor consists of a 200-nm-thick Bi film prepared at RT on a polyimide foil and is applied to different sample holders with defined curvatures (inset). The change of the sensitivity of the sensor with bending radii is shown as an inset graph.

density) normalized to the value of the supply current. First, we note that the samples prepared on polyimide and PEEK foils qualitatively behave in the same way (**Figure 3**a), although the performance on polyimide is better. The deposition of the Bi film on flexible membranes at elevated temperatures has a strong influence on the resulting Hall sensitivity of the device. In particular, the preparation of a 100-nm-thick Bi thin film on polyimide foils at 150 °C allows the sensitivity to be increased by a factor of 2.8, compared with the samples prepared at RT, reaching a remarkable value of –1 V $(AT)^{-1}$ (Figure 3a). A qualitatively similar result is obtained for Bi-based sensors on PEEK foils, although a slightly smaller increase of the sensitivity of 1.9 times is achieved (Figure 3a and Table S1, Supporting Information). We found that sensors deposited at 150 °C on flexible foils show a better performance than their rigid counterparts prepared on Si wafers. For rigid substrates, the maximum sensitivity of –0.6 V $(AT)^{-1}$ was obtained for a 100-nm-thick sensor prepared at RT. The deposition at 100 °C results in a lowering of the Hall sensitivity, due to partial dewetting of the thin Bi film on the Si wafer. The electrical contact is lost for the sample prepared on a Si wafer at 150 °C.

Figure 3b shows the modification of the performance of the Bi Hall sensors prepared on PEEK foils with the thickness of the Bi film. As the current density is increasing with the decrease of the film thickness, the sensitivity is increasing for thinner sensors reaching a maximum of about –0.4 V $(AT)^{-1}$ for the sensor with a 280-nm-thick Bi layer. However, the sensitivity drops when the thickness of the Bi film is reduced below 200 nm. We attribute this finding to the modification of the morphology of the thin Bi films. Indeed, SEM images (Figure 2) reveal a substantial increase of the granularity of the film for a small thickness of Bi below 200 nm. This modification of the film morphology results in a substantial increase of the sensor resistance (Figure S4, Supporting Information). The latter is related to the enhanced scattering probability of the electrons at the grain boundaries when the mean free path of the electrons in Bi becomes comparable to the dimensions of the grains.

Significant improvement of the sensor performance can be achieved by applying post-annealing to the samples prepared at RT. A comparison of the performance of as-prepared and post-annealed sensors is shown in Figure 3c. Treating 230-nm-thick Bi film prepared on polyimide foils at 250 °C for 3 h in air leads to a strong increase of sensitivity up to –(2.29 ± 0.01) V $(AT)^{-1}$, which corresponds to the bulk value of –(2.2–2.6) V $(AT)^{-1}$ recalculated for a Bi film of the same thickness.[23] A similar sensitivity of –2 V $(AT)^{-1}$ of the nano-structured bismuth sensors fabricated for scanning Hall microscopy on plastic cantilevers made of SU-8 was previously reported by Boero et al.[27]

Although the sensors are prepared on polymeric membranes, they are operational in a wide temperature range. The temperature dependence of the Hall response (Figure S5, Supporting Information) shows that the sensors are stable in a consumer temperature range (from –20 °C to 80 °C) with a temperature coefficient of the sensor's sensitivity of about 1 mV (A T K)$^{-1}$.

To investigate their bending performance, flexible sensor elements were mounted on sample holders with concave curvatures of radii varying from 32 mm down to 6 mm. From geometric considerations, these curvatures correspond to strain values in the bismuth film of 0.24% and 1.25%, respectively. Unbent, the sensor reveals a sensitivity of –(0.54 ± 0.01) V (AT)$^{-1}$, which corresponds to the maximum value for the as-prepared sensing elements on the polyimide foils (200-nm-thick Bi film). The sensor response was measured in the planar, bent and then again in the planar arrangement for each radius of curvature (Figure 3d, inset). In the flat state, the sensor response remained at the initial sensitivity even after bending into a radius of 6 mm. We did not observe any degradation in sensor performance even after 50 bending cycles to a radius of 8 mm. For smaller radii, only a minor decay in sensitivity is observed (Figure 3d) and the performance remains at a high value of about –0.47 V (AT)$^{-1}$, which is recovered in full after the sensor is re-measured in the flat arrangement (inset in Figure 3d).

In conclusion, we fabricated flexible bismuth Hall sensors on polymeric PEEK and polyimide foils and identified key optimization procedures which are required to boost the sensitivity of the flexible sensors to the bulk value. The sensor can be bent around the wrist or positioned on the finger to realize an interactive pointing device that visualizes the relative position of the finger with respect to a magnetic field, thus creating a unique feedback element for wearable electronics. The optimized sensors possess a remarkable sensitivity of about –2.3 V (AT)$^{-1}$. We demonstrated that flexible sensors withstand severe mechanical deformations and can be bent into radii of 6 mm with only a minor reduction in sensor performance. Moreover, no degradation of the sensor performance was observed after 50 bending cycles.

Apart from flexible and wearable consumer electronics, thin and bendable Hall sensors are of great interest for integration into electrical machines and drives. Featuring a flat and flexible design, they can be positioned inside the typically curved and narrow (<500 µm) air gaps between rotor and stator (Figure S2 and S3, Supporting Information), in order to provide a direct magnetic field measurement, which is not feasible with current chip-based rigid sensing elements. Such measurements are especially useful for the optimization of eMotor designs and for the rapidly developing market of eMobility, since they help to improve the dynamical performance (stiffness and damping) as well as the positioning accuracy of magnetic bearing systems.[28,29]

Experimental Section

Fabrication of Hall Sensors on Polyimide and PEEK Foils: The structuring processes were carried out by means of optical lithography and lift-off techniques. A commercial image reversal resist (AZ 5214 E) was spun onto the flexible substrate (4000 rotations per min, 35 s). The resist was dried in a convection oven at a temperature of 90–95 °C for 30 min. The resist was exposed at 365 nm, 275 W for 2 s. After that, a reversal bake process was realized at 120 ± 2 °C for 20 min. The baked photoresist is flood exposed (no mask) for 30 s and developed using AZ 726 MIF for 90 s. With this procedure, a profile with overhanging lips is realized in the photoresist layer. The flexible substrate was covered by a Cr(5 nm)/Au(50 nm) layer using thermal evaporation process with deposition rates of 0.1 nm s^{-1} and 0.3 nm s^{-1} for Cr and Au, respectively. In a second lithography run, a lift-off mask for the Bi Hall-cross is realized. These patterned flexible foils were introduced in the sputter deposition chamber, where bismuth films of different thickness ranging from 65 up to 2000 nm were grown (base pressure in the chamber: 10^{-7} mbar; deposition rate: 0.5 nm s^{-1}; Ar was used as a sputter gas at a partial pressure of 1×10^{-3} mbar). The deposition of Bi films was carried out at room temperature or at elevated temperatures up to 150 °C, as stated in the text.

Fabrication of Hall Sensors on Commercial FPCs: Here we used commercially available 150-µm-thick double layer flexible polyimide-based FPCs with a conductor path that defines the cross-shape of the Hall elements. FPC layouts for single Hall elements (Figure S2, Supporting Information), as well as for 1D sensor arrays (Figure 1f) were designed and purchased. First, we deposit a 5-nm-thick Cr adhesive layer onto the FPCs and copper contacting pads (wire thickness of 35 µm) to assure a good adhesion of Bi films to the polymeric membranes. Afterwards, Bi layers are grown at room temperature using magnetron sputter deposition (base pressure: 10^{-7} mbar; Ar sputter pressure: 10^{-3} mbar; sputter rate: 0.5 nm s^{-1}). Both Cr and Bi films are deposited through the opening in the top layer of the FPC as shown in the inset of Figure S2a in the Supporting Information. Using this fabrication method, the electrical contacting of the Bi sensing element is directly established during the deposition process. The thickness of the Bi layers is chosen to 2 µm, to ensure the reliability of the contacts.

Temperature Dependence of Hall Response: The temperature dependence of the Hall response is one of the crucial parameters characterizing the performance of the sensor. The Hall effect in bismuth, as well as in any metallic or semiconducting material is temperature dependent, mainly due to a reduction of the charge carrier mobility with heat in a conductor. Figure S5 in the Supporting Information shows the series of Hall responses from a 2-µm-thick Bi Hall cross prepared on PEEK measured at different temperatures by means of a Peltier element. As typically observed for the Hall effect, the sensitivity of the sensors becomes smaller with an increasing temperature due to the mobility decrease of the charge carriers. The slope of the linear fit shown in the inset provides a value of the temperature coefficient of the sensor's sensitivity of about 1 mV (A T K)$^{-1}$. The temperatures in this investigation represent a realistic operation range for industrial and consumer electronics.

Acquisition Board for Magnetic Pointing Device: The contact end of the sensor was glued to a copper clad laminated with 4 predefined conductors to match the wiring of the sensor. The electrical connection was realized by a silver paste. The sensor module was connected to the acquisition device (Figure S1, Supporting Information) using a 4-wire flat ribbon cable in 4-point measurement configuration. The sensor's response to an applied magnetic field was detected by measuring the variation in the Hall voltage while approaching a NdFeB magnet. The sensor was biased by a constant current of 17 mA (I_{sens}, Figure S1, Supporting Information), supplied by a constant current generator circuit implemented directly on the acquisition device. The voltage signal from the sensor was amplified by an instrumentation amplifier (Amp. 1) with a gain defined by resistance R_1 (Figure S1, Supporting Information). Then, the signal passes to the two cascade amplifier based on two operation amplifiers OPA354. Offset and gain of each cascade can be tuned (R_3, R_{off1}, R_5, R_{off2}, Figure S1, Supporting Information) in order to fit the sensor signal to an input range of the analog to digital converter (ADC) embedded in a microcontroller unit (MCU) C8051F342 of the acquisition device. The acquired data was processed in the MCU and displayed on a bar of 8 light emitting diodes (LEDs), representing

the detection of proximity between the magnetic sensor placed on the finger and the magnet.

Application Potential for Electrical Machines and Drives: Flexible Hall sensors are of great interest not only in the field of consumer electronics. In the rapidly developing market of eMobility there is a strong demand for novel sensor solutions fulfilling specific requirements to pave the way toward more energy efficient and eco-friendly designs of electrical machines. This mainly requires the measurement of the magnetic fields in curved and tiny air gaps (typically <500 μm) between the rotor and stator. In order to accomplish this task, sensor solutions based on the Hall effect have to be developed, which are less than 200 μm thick and flexible. Their realization opens up new fields of application in electrical machines and drives, where conventional rigid semiconductor-based Hall sensors fail. Using the sensor signal as a feedback in control algorithms of active magnetic bearings (AMBs), an improvement of the dynamical performance (stiffness and damping) as well as a more precise positioning accuracy of the magnetic levitation can be achieved.[28,29] Furthermore, the mentioned flux based control of active magnetic bearings can reduce fabrication costs, by replacing expensive position sensing systems,[30] or increase their reliability as a backup control for maintenance-critical off-shore and space applications or in implanted cardiac supporting blood pumps.

To demonstrate the full potential of our technological platform in this respect, we prepared an industry-ready prototype of the Hall sensors onto commercially available polyimide-based double layer FPCs as shown in Figure S2a,b in the Supporting Information. The sensor is mounted to the curved surfaces of the stator poles of an electrical motor (Figure S2c, Supporting Information) or active magnetic bearing (Figure S3, Supporting Information), i.e., into the narrow air gap between rotor and stator (Figure S3a, Supporting Information).

The flexible Hall sensors are employed to monitor the magnetic flux density in a two-axes active magnetic bearing setup (Figure S3b–d, Supporting Information). Figure S5d in the Supporting Information shows the magnetic bearing test setup consisting of the 2-axes radial AMB, a position measurement system, mechanical touch-down bearing as well as an asynchronous motor to drive the system. Designed with a typical magnetic air gap of 500 μm and a stator pole surface of 20 mm × 10 mm the AMB generates forces up to 460 N. Table S2 in the Supporting Information, summarizes the characteristic parameters of the magnetic bearing. Integrated NdFeB magnets provide a permanent magnetic bias allowing a linearized control characteristic of the AMB by differentially connected flux paths of bias and control flux densities (Figure S3a, Supporting Information). Figure S3f, Supporting Information, exemplifies the change of the magnetic flux density in the air gap when the rotor was gradually displaced from the initial position. The corresponding measurement of the rotor position, carried out using a capacitive sensor providing a resolution of about 50 nm, is shown, highlighting that the Hall signal shows the response according to the ramp function of the rotor movements. The presented data and the impressive sensitivity of up to 4 V T^{-1} after amplification together with a resolution of 5 mT in the full range up to 2.3 T demonstrate the potential suitability of flexible bismuth Hall sensors to be applied for flux density measurements in magnetic bearings and electrical machines. Similar measurements were successfully performed using patterned sensors on polyimide foils (Figure 1a).

Supporting Information

Supporting Information is available from the Wiley Online Library or from the author.

Acknowledgements

The authors thank Prof. Wilfried Hofmann (EMA, TU Dresden) for the access to the active magnetic bearing setups, C. Krien (IFW Dresden) for the sputter deposition of Bi films. This work is financed in part via the German Research Foundation DFG (Project Nos. HO 1483/64–1 and SCHM 1298/15–1), BMBF project Nanett (federal research funding of Germany FKZ: 03IS2011F) as well as by the European Research Council within the European Union´s Seventh Framework Programme (FP7/2007–2013)/ERC Grant Agreement No. 306277 and ERC Proof-of-Concept Grant No. 620205.

Received: November 3, 2014
Revised: November 20, 2014
Published online: December 18, 2014

[1] M. G. Lagally, *MRS Bull.* **2007**, *32*, 57.
[2] J. A. Rogers, M. G. Lagally, R. G. Nuzzo, *Nature* **2011**, *477*, 45.
[3] D. H. Kim, J. H. Ahn, W. M. Choi, H. S. Kim, T. H. Kim, J. Z. Song, Y. G. Y. Huang, Z. J. Liu, C. Lu, J. A. Rogers, *Science* **2008**, *320*, 507.
[4] G. A. Salvatore, N. Munzenrieder, T. Kinkeldei, L. Petti, C. Zysset, I. Strebel, L. Buthe, G. Troster, *Nat. Commun.* **2014**, *5*, 2982.
[5] C. L. Wang, H. L. Dong, W. P. Hu, Y. Q. Liu, D. B. Zhu, *Chem. Rev.* **2012**, *112*, 2208.
[6] S. W. Bedel, K. Fogel, P. Lauro, D. Shahrjerdi, J. A. Ott, D. Sadana, *J. Phys. D: Appl. Phys.* **2013**, *46*, 152002.
[7] M. Melzer, D. Makarov, A. Calvimontes, D. Karnaushenko, S. Baunack, R. Kaltofen, Y. F. Mei, O. G. Schmidt, *Nano Lett.* **2011**, *11*, 2522.
[8] D. Karnaushenko, D. Makarov, C. Yan, R. Streubel, O. G. Schmidt, *Adv. Mater.* **2012**, *24*, 4518.
[9] D. H. Kim, N. S. Lu, R. Ma, Y. S. Kim, R. H. Kim, S. D. Wang, J. Wu, S. M. Won, H. Tao, A. Islam, K. J. Yu, T. I. Kim, R. Chowdhury, M. Ying, L. Z. Xu, M. Li, H. J. Chung, H. Keum, M. McCormick, P. Liu, Y. W. Zhang, F. G. Omenetto, Y. G. Huang, T. Coleman, J. A. Rogers, *Science* **2011**, *333*, 838.
[10] R. F. Shepherd, F. Ilievski, W. Choi, S. A. Morin, A. A. Stokes, A. D. Mazzeo, X. Chen, M. Wang, G. M. Whitesides, *Proc. Natl. Acad. Sci. USA* **2011**, *108*, 20400.
[11] S. Bauer, S. Bauer-Gogonea, I. Graz, M. Kaltenbrunner, C. Keplinger, R. Schwödiauer, *Adv. Mater.* **2014**, *26*, 149.
[12] D.-H. Kim, J. Viventi, J. J. Amsden, J. Xiao, L. Vigeland, Y.-S. Kim, J. A. Blanco, B. Panilaitis, E. S. Frechette, D. Contreras, D. L. Kaplan, F. G. Omenetto, Y. Huang, K.-C. Hwang, M. R. Zakin, B. Litt, J. A. Rogers, *Nat. Mater.* **2010**, *9*, 511.
[13] D.-H. Kim, R. Ghaffari, N. Lu, S. Wang, S. P. Lee, H. Keum, R. D'Angelo, L. Klinker, Y. Su, C. Lu, Y.-S. Kim, A. Ameen, Y. Li, Y. Zhang, B. de Graff, Y.-Y. Hsu, Z. J. Liu, J. Ruskin, L. Xu, C. Lu, F. G. Omenetto, Y. Huang, M. Mansour, M. J. Slepian, J. A. Rogers, *Proc. Natl. Acad. Sci. USA* **2012**, *109*, 19910.
[14] W. H. Yeo, Y. S. Kim, J. Lee, A. Ameen, L. K. Shi, M. Li, S. D. Wang, R. Ma, S. H. Jin, Z. Kang, Y. G. Huang, J. A. Rogers, *Adv. Mater.* **2013**, *25*, 2773.
[15] M. Kaltenbrunner, M. S. White, E. D. Glowacki, T. Sekitani, T. Someya, N. S. Sariciftci, S. Bauer, *Nat. Commun.* **2012**, *3*, 770.
[16] M. Kaltenbrunner, T. Sekitani, J. Reeder, T. Yokota, K. Kuribara, T. Tokuhara, M. Drack, R. Schwodiauer, I. Graz, S. Bauer-Gogonea, S. Bauer, T. Someya, *Nature* **2013**, *499*, 458.
[17] S. W. Hwang, H. Tao, D. H. Kim, H. Y. Cheng, J. K. Song, E. Rill, M. A. Brenckle, B. Panilaitis, S. M. Won, Y. S. Kim, Y. M. Song, K. J. Yu, A. Ameen, R. Li, Y. W. Su, M. M. Yang, D. L. Kaplan, M. R. Zakin, M. J. Slepian, Y. G. Huang, F. G. Omenetto, J. A. Rogers, *Science* **2012**, *337*, 1640.
[18] S. Bauer, M. Kaltenbrunner, *ACS Nano* **2014**, *8*, 5380.
[19] A. Sandhu, H. Masuda, A. Oral, J. Bending, *Jpn. J. Appl. Phys.* **2001**, *40*, 524.

[20] A. Sandhu, H. Masuda, A. Oral, S. J. Bending, A. Yamada, M. Konagai, *Ultramicroscopy* **2002**, *91*, 97.
[21] R. Koseva, I. Mönch, J. Schumann, K.-F. Arndt, O. G. Schmidt, *Thin Solid Films* **2010**, *518*, 4847.
[22] R. Koseva, I. Mönch, D. Meier, J. Schumann, K.-F. Arndt, L. Schulz, B. Zhao, O. G. Schmidt, *Thin Solid Films* **2012**, *520*, 5589.
[23] a) C. Kittel, *Introduction to Solid State Physics*, 4th ed., John Wiley & Sons, Inc, New York **1971**; b) P. Nording, J. Österman, *Physics Handbook*, Chartwell-Bratt Ltd., Bromley, UK **1987**.
[24] Room temperature Hall coefficient and resistivityfor selected chemical elements, http://it.stlawu.edu/~koon/HallTable.html, accessed: **December 2014**.
[25] D. E. Beutler, N. Giordano, *Phys. Rev. B* **1988**, *38*, 8.
[26] F. H. Yang, K. Liu, K. M. Hong, D. H. Reich, P. C. Searson, C. L. Chien, *Science* **1999**, *284*, 1335.
[27] S. Mouaziz, S. Boero, L. Scandella, R. Popovic, J. Brugger, presented at "Trends in Nanotechnology"(TNT 2004), Reference: LMIS1-POSTER-2007-033, Segovia, Spain, **2004**; see http://infoscience.epfl.ch/record/101340?ln=en, accessed: December 2014.
[28] X. Chen, K. Lie, K. Xiao, in *Proc. 11th Int. Symp. Magnetic Bearings (ISMB)*, Nara, Japan, **2008**, pp. 455–461
[29] J. H. Yi, K. H. Park, S. H. Kim, Y. K. Kwaik, M. Abdelfatha, I. Busch-Vishniac, in *Proc. 34th IEEE Conf. on Decision and Control*, **1995**, *3*, pp. 2153.
[30] H. Bleuler, D. Vischer, G. Schweitzer, A. Traxler, D. Zlatnik, *Automatica* **1995**, *30*, 871.